Eur. Phys. J. Plus (2023) 138:178
https://doi.org/10.1140/epjp/s13360-023-03773-0

THE EUROPEAN PHYSICAL JOURNAL PLUS

Regular Article

On soft gluon resummation for associated single top production with a Higgs boson at the LHC

Anna Kulesza[1,a], **Laura Moreno Valero**[1,b], **Vincent Theeuwes**[2,c]

[1] Institute for Theoretical Physics, WWU Münster, 48149 Münster, Germany
[2] Institute for Theoretical Physics, Georg-August-Univesity Göttingen, Friedrich-Hund-Platz 1, 37077 Göttingen, Germany

Received: 17 October 2021 / Accepted: 6 February 2023

Abstract We investigate threshold resummation of soft gluon corrections for the *s*-channel process of a single top quark production in association with a Higgs boson in the Standard Model. We choose to work in the three-particle invariant mass kinematics in direct QCD, i.e. in the space of Mellin moments. Our results take into account terms of up to next-to-leading logarithmic (NLL) precision, as well as $\mathcal{O}(\alpha_s)$ non-logarithmic terms which do not vanish at threshold. After presenting analytical expressions, we discuss the corresponding numerical results for the total cross section and the invariant mass distribution at the LHC.

1 Introduction

The Higgs boson interactions with top quarks and electroweak gauge bosons are one of the most important subjects of studies at the LHC. The strength of the top-Higgs Yukawa coupling can be probed directly without making any assumptions on its nature in the associated production processes involving both a top quark and a Higgs boson in the final state. Alongside the intensively studied associated production with a top-antitop quark pair, $t\bar{t}H$, the associated process of a single top quark and a Higgs boson (tH) production has been attracting a lot of attention lately. Although in the Standard Model (SM) the tH production rate at the LHC is only one tenth of the rate for the $t\bar{t}H$ production, the process is of great interest. It offers a unique possibility to directly measure not only the value of the Yukawa coupling but also a relative sign between it and the coupling of a Higgs boson to a W boson [1–3]. The tH cross section receives contributions from diagrams with H radiated by the t quark as well as from diagrams with H radiated by the W boson. The value of the cross section depends strongly on the interference between these diagrams. In fact, it is the interference between diagrams involving the two couplings that is responsible for the small value of the cross section in the SM. For the same reason the tH process offers a very sensitive probe of new physics interactions. The small cross section notwithstanding, first experimental searches for the process have been already conducted at the LHC [4, 5] and the rate for H boson production in the tH process is included in the measurements together with the $t\bar{t}H$ process [6–8].

Given on one side the importance of the tH production for new physics searches and, on the other side, much larger statistical samples and expected better understanding of the systematic uncertainties of the future LHC measurements, the precision with which the theoretical predictions are known becomes a central issue. At lowest order in perturbation theory, the production mechanisms for the associated production of the Higgs boson with a single top quark can be classified according to the virtuality of a W, which is either exchanged or emitted in the process. Correspondingly, the three mechanisms are the t-channel ($qb \to tHq'$), s-channel ($q\bar{q}' \to tH\bar{b}$) and the tW associated channel ($gb \to tHW$). Strictly speaking, this classification is only valid assuming five active quark flavours, i.e. in the so-called five-flavour scheme (5FS) which involves b quarks in the initial state. In the four-flavour scheme (4FS), initial state b-quarks can only appear as a result of a $g \to b\bar{b}$ splitting. First calculations of the next-to-leading order (NLO) QCD correction for the t-channel (in 4FS and 5FS) and s-channel production in the SM were reported in [9], whereas an analysis of the NLO QCD corrections to the t-channel process in the framework of SM Effective Field Theory (SMEFT) was undertaken in [10]. Recently, NLO QCD+EW precision for the tHj production was reached in the combined analysis of all channels in 5FS [11].

With the full NNLO calculations being technically out of reach for the $2 \to 3$ processes considered here, a question remains if at least some part of the higher order corrections can be investigated already now. Higher-order corrections due to soft gluon emissions provide a class of corrections which can be identified and accounted for in a systematic manner, as shown in the case of the $t\bar{t}H$ or $t\bar{t}Z/W$ production [12–22]. In particular, it has been reported in [14–16], that adding soft gluon corrections calculated at the next-to-next-to-leading-logarithmic (NNLL) accuracy leads to a significant reduction of the scale uncertainty and a correction to

[a] e-mail: anna.kulesza@uni-muenster.de (corresponding author)
[b] e-mail: l_more02@uni-muenster.de
[c] e-mail: vtheeuwe@gmail.com

Published online: 26 February 2023

the $t\bar{t}H$ or $t\bar{t}Z$ total cross section of up to 20%, depending on the choice of the central scale. Of course, one cannot expect a similar conclusion to automatically apply to the single associated top production, as for example the initial state and final state partons are different in both cases. In particular, in contrast to the tH production, the $t\bar{t}H$ process involves the gluon-gluon channel, so it is reasonable to expect smaller impact of soft gluon corrections in the former case. Nevertheless, since the processes are often analysed together by the experiments, theoretical predictions for the two processes should be known with the same accuracy. In a similar, in this respect, case of the associated heavy gauge boson production, the $t\bar{t}W$ process, taking place at LO only in the quark channel, is known at the NLO+NNLL accuracy, i.e. the same level of accuracy as reached for the $t\bar{t}Z$ process.

So far, only the predictions for the t-channel tH production have been considered in the context of soft gluon emission. More specifically, in [23, 24] contributions to the NNLO corrections due to such emission were investigated. That study used the so-called one particle inclusive (1PI) kinematics. Performing full resummed calculations, i.e. obtaining numerical predictions which include soft gluon corrections to all orders in perturbation theory in the direct resummation framework (i.e. in Mellin space) is known to be notoriously difficult in 1PI, see e.g [26]. For processes involving jet production it has been achieved only for inclusive enough quantities [25]. Notably, 1PI threshold resummation for single-inclusive jet production has been carried out in the SCET framework [27].

In this work, we investigate the application of the direct Mellin resummation techniques to the s-channel tH production to which we will from now on refer to as s-channel tHj production. While the contribution from the s-channel to the tHj production is much smaller than the one from the t-channel, it proves a useful setting for an exploratory study. The s-channel does not involve initial state b-quarks and therefore it remains largely insensitive to the FS choice, which is not the case for the t-channel predictions. Given the known problems with performing fully resummed calculations in 1PI kinematics, we focus instead on the three-particle invariant mass kinematics, which has successfully been applied to the production of three massive particles, some carrying colour, in the final state [12–16]. Application of these kinematics to the process in question requires considering kinematical information on a jet j produced together with a top quark and a Higgs boson. This, in turn, brings up the question of an appropriate treatment of the jet. In the presence of particles other than massless partons in the final state at LO, 1PI kinematics allows to perform calculations of observables which do not directly involve the jet by treating it inclusively, i.e. as unobserved. In other words, the threshold variable in 1PI kinematics does not directly involve the momenta of the massless parton. This is not the case in the invariant mass kinematics. Following [28], in this kinematics the jet can be treated as massless or massive at the partonic threshold, leading to different structures of the logarithmic corrections. Massless jet approach results in double logarithmic contributions in the resummed factor describing the jet. Giving up the assumption of a vanishing jet mass at threshold leads to only single logarithmic contributions, albeit with coefficients depending on the jet size parameter. In the following, we consider the impact of threshold corrections on predictions in the massive jet approach. Our resummed results take into account leading logarithmic (LL) and next-to-leading logarithmic (NLL) terms together with $\mathcal{O}(\alpha_s)$ non-logarithmic contributions which do not vanish at threshold.

The rest of the paper is structured as follows: in Section 2 we present the theoretical framework and the corresponding analytical expressions. Section 3 focuses on the numerical predictions. First we discuss the relation between the full NLO cross sections and the expansion of the resummed cross section truncated at NLO. Then we present the resummed NLL predictions matched to the NLO results. Section 4 contains a summary of our results.

2 NLL resummation in the triple invariant mass kinematics: theoretical framework

In the following we consider the corrections due to gluon emissions in the limit of partonic center-of-mass energy $\hat{s}$ approaching the invariant mass Q of the top quark (t), the Higgs boson (H) and the jet (j) , $Q^2 \equiv (p_t + p_H + p_j)^2 \to \hat{s}$. This corresponds to the limit $\hat{\rho} \to 1$ of the threshold variable $\hat{\rho} \equiv Q^2/\hat{s}$. In the s-channel process, the final state jet is initiated by the b-quark. In this work we treat the b quark as massless, i.e. we use a jet function to describe the (quasi-)collinear emission from the final state quark.[1] Note that our definition of threshold in general permits configurations with nonzero invariant jet mass p_j^2 at threshold [28]. As a useful shortcut, we will therefore refer to the final-state jet and its treatment as "massive jet" and "massive jet approach", respectively, in the rest of this work. However, in our set-up the contributing configurations will also involve those with a vanishing jet mass at threshold, as is the case, e.g. at tree level.

In general, the construction of the resummation formalism for a $2 \to 3$ process builds up on the earlier work for the $2 \to 2$ processes [28–31]. Here we adapt the expressions for the $t\bar{t}H(W, Z)$ from [14, 15] to account for the presence of a final state jet instead of a top quark. The factorization of the soft emission, necessary to perform resummation, takes place in Mellin space, where the Mellin moments N of the partonic cross sections are taken w.r.t. the variable $\hat{\rho}$. At the next-to-leading logarithmic (NLL) accuracy, the resummed expression for the partonic cross section has a schematical form

$$\hat{\tilde{\sigma}}_{ij}^{(\mathrm{NLL})} = \mathrm{Tr}\big[\mathbf{H}_{ij\to tHk}\ \mathbf{S}_{ij\to tHk}\big]\Delta_i \Delta_j J_k\,. \tag{1}$$

[1] In the context of gluon emissions, nonzero bottom quark mass would act as a regulator for collinear singularities. Thus singularities originating from emission off the final state would only be of the soft nature, and the corresponding large logarithmic contributions would be included in the soft function.

Since the soft radiation is coherently sensitive to the colour structure of the underlying hard process $ij \to tHk$, the hard function **H**, representing hard off-shell dynamics of the process, and the soft function **S**, describing pure soft radiation, are matrices in color space. The Δ_i jet functions contain logarithmic contributions due to (soft-)colinear radiation from the incoming quarks or antiquarks, while J_k corresponds to the final state jet function describing emissions off a quark k.

In our calculations, following [28], we define the final state jet four-momentum as the sum over the four-momenta of particles flowing into a cone of half-aperture (angular radius) δ around the jet axis. This approach corresponds to the small cone approximation [32, 33] used in jet calculations. In the small cone approximation the δ parameter is related to the jet radius R through $\delta = R/\cosh(\eta)$, where η is the pseudorapidity of the jet. The approximation is known to work very well even up to relatively large values of $R \sim 0.7$ [34, 35].

The incoming jet functions are independent of the process and read

$$\Delta_i = \exp\left[\int_0^1 \mathrm{d}z\, \frac{z^{N-1}-1}{1-z}\left\{\int_{\mu_F^2}^{(1-z)^2Q^2} \frac{dq^2}{q^2} A_i(\alpha_s(q^2))\right\}\right], \tag{2}$$

where μ_F is the factorization scale. The outgoing jet function for massive jets it is given by [28]

$$J_k = \exp\left[\int_{0^1} \mathrm{d}z\, \frac{z^{N-1}-1}{1-z} C_k^{\mathrm{M}}\left(\alpha_{s((1-z)^2Q^2)}\right)\right]. \tag{3}$$

As discussed in [28], the outgoing jet function contains only single logarithms in the case of a non-vanishing jet mass and carries logarithmic dependence on δ which enters through the coefficient C_k^{M}. The coefficients A_i, C_i^{M} are perturbative series in α_s,

$$F_i = \frac{\alpha_s}{\pi} F_i^{(1)} + \frac{\alpha_s^2}{\pi^2} F_i^{(2)} + \dots,$$

with F_i standing in for any of the coefficients. In order to achieve the NLL accuracy, $A_i^{(1)}$, $A_i^{(2)}$ and $C_i^{\mathrm{M},(1)}$ are needed. At LO, the tHj production involves only quarks in the initial and final state, i.e. $i = q$. The LL $A_q^{(1)}$ coefficient as well as the NLL $A_q^{(2)}$ coefficient of the incoming quark jet function are well known [36, 37]

$$A_q^{(1)} = C_F, \qquad A_q^{(2)} = \frac{1}{2} C_F K \quad \text{with} \quad K = C_A\left(\frac{67}{18} - \frac{\pi^2}{6}\right) - \frac{5}{9} N_f\,. \tag{4}$$

For the outgoing jet function, our calculations return

$$C_q^{\mathrm{M},(1)} = C_F \log\left(\frac{Q^2}{\delta^2 E_q^2}\right), \tag{5}$$

with the δ dependence entering logarithmically, as expected.

The function **S** sums logarithmic contributions from soft wide-angle emission. In Eq. (1) it is already rescaled by the inverse of the soft function contributions for the incoming and outgoing lines, to avoid double counting of soft contributions included in the Δ_i and J_k functions used in this work. In the most general case, the solution of the evolution equation for **S** [28] involves path-order exponentials of the integrals over the soft anomalous dimension $\mathbf{\Gamma} = \frac{\alpha_s}{\pi}\mathbf{\Gamma}^{(1)} + \dots$. To reach the NLL accuracy, we need to know the one-loop soft anomalous dimension $\mathbf{\Gamma}^{(1)}$. For the process $q\bar{q}' \to tHk$ with $q, \bar{q}', k$ corresponding to massless quark lines we find

$$\begin{aligned}\Gamma^{(1)}_{q\bar{q}'\to tHk} = {} & C_F \mathbb{1}\left[\log\left(\frac{s_{tk}-m_t^2}{m_t Q}\right) - \frac{1}{2}(1-i\pi)\right] \\ & - \frac{1}{2}\boldsymbol{C_I}\left[\log\left(\frac{s_{tk}-m_t^2}{m_t Q}\right) - \log\left(\frac{t_{qk}\left(t_{\bar{q}'t}-m_t^2\right)}{m_t Q^3}\right)\right] \\ & - \mathbf{T}_{qt}\log\left(\frac{t_{\bar{q}'k}\left(t_{qt}-m_t^2\right)}{t_{qk}\left(t_{\bar{q}'t}-m_t^2\right)}\right),\end{aligned} \tag{6}$$

where we have $s_{ij} = (p_i + p_j)^2$, $t_{ij} = (p_i - p_j)^2$, $\boldsymbol{C_I} = \mathrm{Diag}(0, C_A)$ and

$$\mathbf{T}_{qt} = \begin{pmatrix} 0 & -\frac{C_F}{2C_A} \\ -1 & -2C_F + \frac{C_A}{2} \end{pmatrix} \tag{7}$$

or

$$\mathbf{T}_{q\bar{t}} = \begin{pmatrix} 0 & \frac{C_F}{2C_A} \\ 1 & 2C_F - C_A \end{pmatrix} \tag{8}$$

for the $q\bar{q}' \to \bar{t}Hk$ process. Our results for $\mathbf{\Gamma}^{(1)}$ are obtained in the singlet-octet s-channel basis and agree with the result recently published in the literature [23].

Apart from knowing the soft anomalous dimension, evaluation of the soft function at any scale also requires knowing the boundary condition $\tilde{\mathbf{S}}$ in the solution of the renormalization group equation at $\mu_R = Q/\bar{N}$, with $\bar{N} = Ne^{\gamma_E}$ and γ_E the Euler constant, cf. Eq. (13) below. $\tilde{\mathbf{S}}$ is a purely eikonal function which can be calculated perturbatively

$$\tilde{\mathbf{S}} = \tilde{\mathbf{S}}^{(0)} + \frac{\alpha_s}{\pi}\tilde{\mathbf{S}}^{(1)} + \dots \tag{9}$$

The leading-order soft function is given by

$$\tilde{\mathbf{S}}^{(0)} = \begin{pmatrix} C_A^2 & 0 \\ 0 & \frac{C_A C_F}{2} \end{pmatrix}. \tag{10}$$

With $\tilde{\mathbf{S}}^{(0)}$ and $\mathbf{\Gamma}^{(1)}$, NLL precision can be reached. Any higher precision requires also the expression for $\tilde{\mathbf{S}}^{(1)}$. For massless initial state $i = q, \bar{q}'$ and final state k quarks we obtain finite contributions in the form

$$\begin{aligned} \tilde{\mathbf{S}}^{(1)} = \tilde{\mathbf{S}}^{(0)}\big\{ & C_F \mathbb{1}[S_{tt} - 2S_{tk}] + \boldsymbol{C_I}\big[S_{q\bar{q}'} + S_{tk} - S_{qk} - S_{\bar{q}'t}\big] \\ & + 2\mathbf{T}_{qt}\big[S_{qt} + S_{\bar{q}'k} - S_{qk} - S_{\bar{q}'t}\big]\big\} \end{aligned} \tag{11}$$

with

$$\begin{aligned} S_{q\bar{q}'} &= -\frac{\pi^2}{12} \\ S_{tt} &= \frac{1}{2\beta_t}\log\left(\frac{1+\beta_t}{1-\beta_t}\right) \\ S_{tk} &= -\frac{\pi^2}{24} + \frac{1}{8}\log^2\frac{1+\beta_t}{1-\beta_t} \\ &\quad + \frac{1}{2}\left\{\mathrm{Li}_2\left(1 - \frac{2E_tE_k(1-\beta_t)}{s_{tk}-m_t^2}\right) + \mathrm{Li}_2\left(1 - \frac{2E_tE_k(1+\beta_t)}{s_{tk}-m_t^2}\right)\right\} \\ S_{it} &= -\frac{\pi^2}{24} + \frac{1}{8}\log^2\frac{1+\beta_t}{1-\beta_t} \\ &\quad + \frac{1}{2}\left\{\mathrm{Li}_2\left(1 - \frac{E_tQ(1+\beta_t)}{m_t^2-t_{it}}\right) + \mathrm{Li}_2\left(1 - \frac{E_tQ(1-\beta_t)}{m_t^2-t_{it}}\right)\right\} \\ S_{ik} &= -\frac{\pi^2}{12} + \frac{1}{2}\mathrm{Li}_2\left(1 + \frac{2E_kQ}{t_{ik}}\right) \end{aligned} \tag{12}$$

and $\beta_t = \sqrt{1 - m_t^2/E_t^2}$.

Calculations of the soft function in the dimensional regularization (DR) scheme leading to the above results deliver also information on double and single poles in ϵ. The one-loop soft function corresponding to $\tilde{\mathbf{S}}^{(1)}$ does not contain $1/\epsilon^2$ poles, while the coefficients of the $1/\epsilon$ terms return the soft anomalous dimension given in Eq. (6), thus providing an additional check of our calculations.

In order to simplify the solution of the renormalization group equation for the soft function, and, correspondingly, the expression in Eq. (1), we write it in the color basis in which the one-loop soft anomalous dimension $\mathbf{\Gamma}^{(1)}$, driving the evolution of the soft-function, is diagonal. We denote all matrices in this basis with the subscript R. The IJ element of the diagonalised one-loop soft anomalous dimension is thus

$$\mathbf{\Gamma}^{(1)}_{R,IJ} = \lambda_I^{(1)}\delta_{IJ}$$

where $\lambda_I^{(1)}$ are the eigenvalues of $\mathbf{\Gamma}^{(1)}$. The soft function has then the form

$$\mathbf{S}_{R,IJ} = \tilde{\mathbf{S}}_{R,IJ}\exp\left[\frac{\log(1-2\lambda)}{2\pi b_0}\left(\left(\lambda_I^{(1)}\right)^* + \lambda_J^{(1)}\right)\right], \tag{13}$$

with $\lambda = \alpha_s(\mu_R^2)b_0\log N$, $b_0 = (11C_A - 2nf)/(12\pi)$ and μ_R the renormalization scale.

The NLL precision of the resummed expression can be increased by including the $\mathcal{O}(\alpha_s)$ terms in the expansions of the hard function $\mathbf{H} = \mathbf{H}^{(0)} + \frac{\alpha_s}{\pi}\mathbf{H}^{(1)} + \dots$ and the soft function $\tilde{\mathbf{S}}$, cf. Eq. (9), as well as collinear non-logarithmic contributions. In the literature on direct QCD resummation such terms are often collectively referred to as the "$\mathbf{C}^{(1)}$" coefficient. We will refer to the

precision obtained by adding the information on $\mathbf{C}^{(1)}$ to the NLL result as "NLL′" [2] and give the corresponding expressions below. In the $R-$basis we have

$$\begin{aligned}\frac{d\tilde{\hat{\sigma}}_{ij}^{(\mathrm{NLL}')}}{dQ^2}(N, Q^2, \{m^2\}, \mu_\mathrm{F}^2, \mu_\mathrm{R}^2) = \\ (\mathbf{H}_{R,IJ}\tilde{\mathbf{S}}_{R,JI})(Q^2, \{m^2\}, \mu_\mathrm{F}^2, \mu_\mathrm{R}^2, \delta) \\ \times\Delta_i(N+1, Q^2, \mu_\mathrm{F}^2, \mu_\mathrm{R}^2)\Delta_j(N+1, Q^2, \mu_\mathrm{F}^2, \mu_\mathrm{R}^2) \\ \times J_k(N+1, \delta, Q^2, \mu_\mathrm{R}^2)\,\exp\left[\frac{\log(1-2\lambda)}{2\pi b_0}\left(\left(\lambda_J^{(1)}\right)^* + \lambda_I^{(1)}\right)\right],\end{aligned} \tag{14}$$

where $\{m^2\}$ stands for a set of mass parameters characteristic for the process. The NLL′ precision is achieved with

$$\begin{aligned}\mathbf{H}_R\,\tilde{\mathbf{S}}_R &= \mathbf{H}_R^{(0)}\tilde{\mathbf{S}}_R^{(0)}\left(\mathbb{1} + \frac{\alpha_\mathrm{s}}{\pi}\,\mathbf{C}_R^{(1)}\right) \\ &= \mathbf{H}_R^{(0)}\tilde{\mathbf{S}}_R^{(0)} + \frac{\alpha_\mathrm{s}}{\pi}\left[\mathbf{H}_R^{(0)}\tilde{\mathbf{S}}_R^{(1)} + \mathbf{V}_R^{(1)}\tilde{\mathbf{S}}_R^{(0)} + \mathbf{H}_R^{(0)}\tilde{\mathbf{S}}_R^{(0)}\left(2\tilde{J}_{in}^{(1)} + \tilde{J}_{out}^{(1)}\right)\right].\end{aligned} \tag{15}$$

If only the $\mathbf{H}_R^{(0)}\tilde{\mathbf{S}}_R^{(0)}$ term, with its trace corresponding to the leading order partonic cross section, is kept in the expression above, the precision of the resummed cross section in Eq. (14) reduces to NLL. Equation (15) defines the NLL′ precision as the NLL precision supplemented with additional information included in the coefficient $\mathbf{C}^{(1)}$. It consists of $\mathcal{O}(\alpha_\mathrm{s})$ contributions from the virtual corrections $\mathbf{V}^{(1)}$, collinear non-logarithmic contributions $\tilde{J}_{in}^{(1)}$ from incoming quark jets, as well as $\mathcal{O}(\alpha_\mathrm{s})$ non-logarithmic contributions $\tilde{J}_{out}^{(1)}$ from the outgoing jets. The virtual corrections $\mathbf{V}^{(1)}$ are calculated numerically using the aMC@NLO code [38], whereas the collinear contributions are calculated analytically. In particular, for the outgoing quark jet with nonzero invariant mass we find the finite non-logarithmic contributions of the form

$$\tilde{J}_{out}^{\mathrm{M},(1)} = C_F\left(2 - \frac{\pi^2}{6} + \frac{1}{4}\log^2\frac{\mu_R^2}{Q^2} + \frac{3}{2}\log\frac{\mu_R}{\delta E_k} - \log^2\frac{2}{\delta} + \log^2\frac{E_k\delta}{Q} - 2\gamma_E\log\frac{Q}{\delta E_k}\right), \tag{16}$$

where k corresponds to a massless final state quark.

Our calculations of the outgoing jet function, leading to Eq. (16) return coefficients of the $1/\epsilon^2$ and $1/\epsilon$ poles corresponding to cusp and non-cusp contributions to the jet anomalous dimension. They also return a single logarithm of N, accompanied by a coefficient logarithmic in δ, as expected for massive jet functions [28].

The numerical predictions in the next section for the resummation-improved hadronic cross sections for the s-channel process $h_1h_2 \to tH + X$ are obtained through matching the NLO cross section with the hadronic equivalent of Eq. (14). In this way, the full information from the NLO calculations is preserved, while double counting of the LO and NLO contributions included in the NLL′ expression is avoided. More specifically,

$$\begin{aligned}\frac{d\sigma_{h_1h_2}^{(\mathrm{NLO+NLL}')}}{dQ^2}(Q^2, \{m^2\}, \mu_\mathrm{F}^2, \mu_\mathrm{R}^2) = \frac{d\sigma_{h_1h_2}^{(\mathrm{NLO})}}{dQ^2}(Q^2, \{m^2\}, \mu_\mathrm{F}^2, \mu_\mathrm{R}^2) \\ + \frac{d\sigma_{h_1h_2}^{(\mathrm{res-exp})}}{dQ^2}(Q^2, \{m^2\}, \mu_\mathrm{F}^2, \mu_\mathrm{R}^2)\end{aligned} \tag{17}$$

with

$$\begin{aligned}\frac{d\sigma_{h_1h_2}^{(\mathrm{res-exp})}}{dQ^2}(Q^2, \{m^2\}, \mu_\mathrm{F}^2, \mu_\mathrm{R}^2) = \sum_{i,j=\{q,\bar{q}'\}}\int_\mathsf{C}\frac{dN}{2\pi i}\,\rho^{-N}\,f_{i/h_1}^{(N+1)}(\mu_\mathrm{F}^2)\,f_{j/h_2}^{(N+1)}(\mu_\mathrm{F}^2) \\ \times\left[\frac{d\tilde{\hat{\sigma}}_{q\bar{q}'}^{(\mathrm{NLL}')}}{dQ^2}(N, Q^2, \{m^2\}, \mu_\mathrm{F}^2, \mu_\mathrm{R}^2) - \frac{d\tilde{\hat{\sigma}}_{q\bar{q}'}^{(\mathrm{NLL}')}}{dQ^2}(N, Q^2, \{m^2\}, \mu_\mathrm{F}^2, \mu_\mathrm{R}^2)|_{(\mathrm{NLO})}\right],\end{aligned} \tag{18}$$

where $d\tilde{\hat{\sigma}}_{q\bar{q}'}^{(\mathrm{NLL}')}/dQ^2|_{(\mathrm{NLO})}$ represents the perturbative expansion of $d\tilde{\hat{\sigma}}_{q\bar{q}'}^{(\mathrm{NLL}')}/dQ^2$ truncated at $\mathcal{O}(\alpha_\mathrm{s})$. The Mellin moments of the parton distribution functions are defined in the usual way as

$$f_{i/h}^{(N)}(\mu_\mathrm{F}^2) = \int_0^1 dx\,x^{N-1}f_{i/h}(x, \mu_\mathrm{F}^2),$$

and the inverse Mellin transform is evaluated using a contour C in the complex N space using the minimal prescription method developed in [41]. The total cross sections are calculated by integrating the invariant mass distribution in Eq. (17) over Q^2.

[2] This accuracy is formally equivalent to the "NLL′" notation used in the SCET literature on resummation. However the subleading terms beyond the nominal accuracy may differ, resulting in numerical differences between the SCET and direct QCD predictions at a given accuracy.

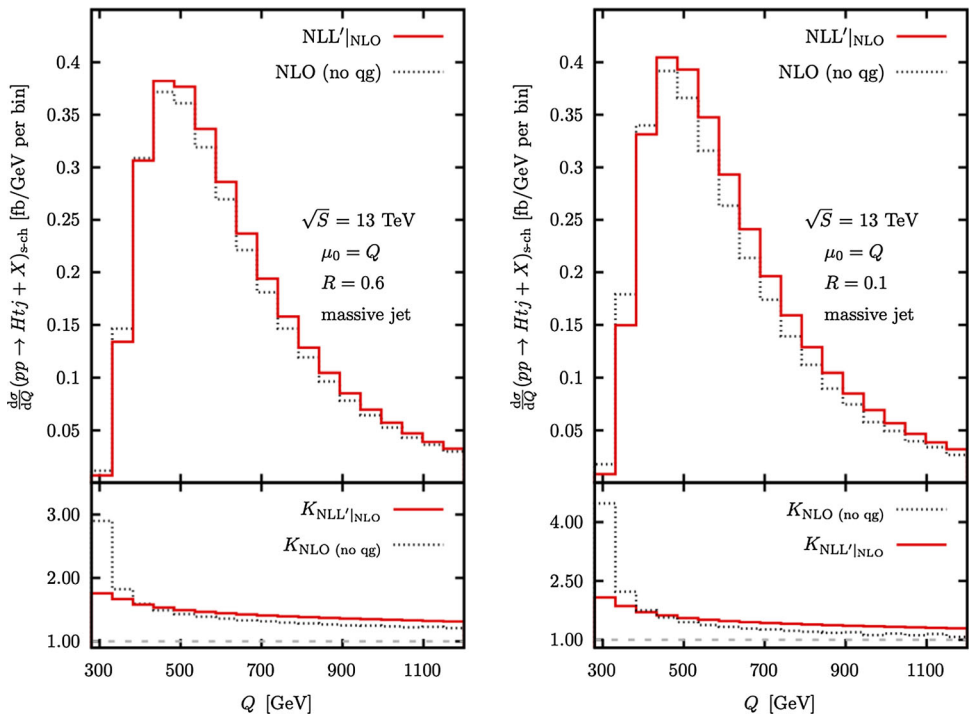

Fig. 1 Differential distributions in Q for massive jets for (left plot) $R = 0.6$ and for (right plot) $R = 0.1$: (top) absolute values of the NLO (no qg), NLL′|$_{\text{NLO}}$ distributions and (bottom) ratios of NLL′|$_{\text{NLO}}$ and NLO (no qg) results to the LO predictions

3 Numerical results

In this section we discuss the results for NLO+NLL′ resummation of soft gluon correction for the s-channel tHj production at the LHC collision energy $\sqrt{S}$=13 TeV. The NLO cross section is calculated using the aMC@NLO code [38] together with the anti-k$_t$ jet algorithm [42]. We use $m_t = 173$ GeV and $m_H = 125$ GeV and employ the MSHT20 parton distribution sets [43]. Unless otherwise stated, the results shown in the plots are obtained for the central scale choice $\mu_{R,0} = \mu_{F,0} = \mu_0 = Q$ and for the jet radius $R = 0.6$.

We begin by investigating how well an expansion of the resummed cross section approximates the NLO cross section. More precisely, we consider the NLO cross section originating from the $q\bar{q}'$ channel, i.e. the NLO cross section with the qg channel removed, which we call "NLO (no qg)". Since the qg channel is subleading in powers of N w.r.t. the $q\bar{q}'$ channel, it cannot be resummed within the current formalism and therefore should not be taken into consideration in the comparison. Given that the threshold definition we use here depends on the variable Q, in the first step we study differential distributions in Q. In the left plot in Fig. 1 we compare the NLO (no qg) distributions with the expansions of the NLL′ cross section up to NLO, called "NLL′|$_{\text{NLO}}$ " for a phenomenologically viable value of the R parameter, $R = 0.6$. For most of the range of Q shown in the plots, the expansion overestimates the NLO (no qg) distribution by around a few percent. Only at the lower end of the spectrum, the expansion underestimates the NLO result but this region is relatively small and does not provide a dominant contribution to the total cross section.

In the right plot in Fig. 1 we study the invariant mass distributions obtained for a smaller value of R, $R = 0.1$. For smaller R, the NLO (no qg) distribution in Q naturally becomes narrower since narrower jets are less massive and the invariant mass of the full system decreases correspondingly. Additionally, we see that the quality of the approximation of the NLO (no qg) result decreases slightly in comparison to the $R = 0.6$ case. The dependence of the NLL′|$_{\text{NLO}}$ results on δ manifests itself in the higher absolute values for these distributions at smaller R. This dependence can be seen as an artefact of our setup, where by choosing the threshold variable dependent on the invariant mass Q, we are forced to define a jet, thus introducing the dependence on δ in the NLL′|$_{\text{NLO}}$ cross sections. The dependence must cancel against δ dependence of the contributions from hard radiation, not included in the soft approximation, in the inclusive NLO cross section.

The lower panels of the plots in Fig. 1 display the ratio of the invariant mass distributions to the LO distribution. We note that the NLO (no qg) corrections are substantial for all values of Q and can be well above 50% for the Q values corresponding to the peak of the distribution. In comparison with the ratios for the NLO (no qg) distributions, the ratios of the NLL′|$_{\text{NLO}}$ to the LO distributions are flatter. This corresponds to the NLL′|$_{\text{NLO}}$ distributions being closer in shape to the LO distributions than the NLO (no qg) distributions, in accordance with the former ones being calculated in the 3-particle kinematics limit. For most of the range of Q shown in the plots, the expansion overestimates the NLO (no qg) distribution by around a few percent. Only at the lower end of the spectrum, the expansion underestimates the NLO result but this region is relatively small and does not provide a dominant contribution to the total cross section.

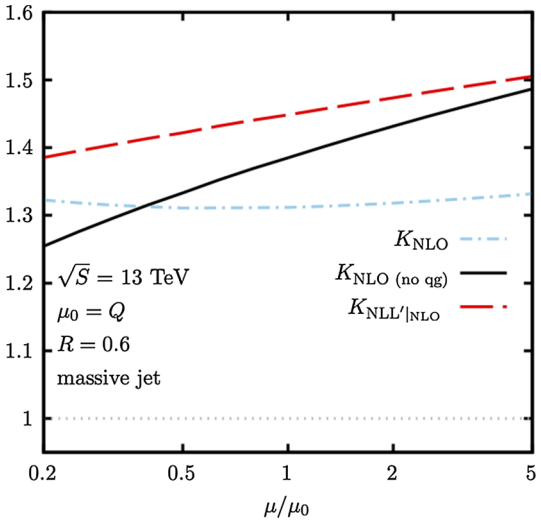

Fig. 2 Total K-factors as a function of μ/μ_0 for $R = 0.6$: ratios of the total cross sections calculated at the NLO, NLO (no qg) and NLL$'|_{\rm NLO}$ accuracy to the LO total cross section

In Fig. 2 we show scale variation for $\mu = \mu_F = \mu_R$ around the central scale $\mu_0 = Q$ of a set of K factors, defined as the ratios of the NLO, NLO (no qg) and NLL$'|_{\rm NLO}$ total cross sections to the LO cross section. First we observe that the full NLO corrections to the total cross section are substantial, above 30% within the range of μ considered here. Figure 2 also shows that most of the NLO cross section is provided by the quark channel, while the NLO qg terms at $\mu/\mu_0 = 1$ provide contributions of above 5% to the full NLO result or of around 25% to the NLO corrections. These contributions are negative for the most of the scale range shown, specifically where the difference between NLO (no qg) and NLO is the most pronounced. As already discussed, in our approach resummation is performed for the dominant $q\bar{q}'$ channel, while the qg channel is included at the NLO accuracy.

The overestimation of the NLO (no qg) results by the NLL$'|_{\rm NLO}$ approximation for most values of Q observed for differential distributions carries over to the total cross sections. On the other hand, the expansions overestimate the NLO (no qg) result by around 3% at $\mu = \mu_0 = Q$. In terms of K-factors, this corresponds to $K_{\rm NLO\ (no\ qg)}$ of around 1.4 at this value of μ, while the expansions provide K-factors of around 1.45, see Fig. 2. The agreement among the K-factors improves significantly as the scale increases, indicating that the scale-dependent terms provide considerable contributions to the NLO (no qg) cross section.

The dependence of the NLO expansions of the resummed cross section on the jet parameter R is plotted in Fig. 3 for the same K-factors as shown in Fig. 2. As R gets smaller, the terms logarithmic in δ become more and more relevant, driving the difference between the expansion of the resummed cross section and the NLO result further apart. However, the dependence on R is relatively mild for moderate R values. Overall, for the central scale choices $\mu_0 = Q$ and a wide range of R values, the NLO (no qg) result differs from the NLL$'|_{\rm NLO}$ expansion by up to a few percent. The increasing difference between the NLO (no qg) and the NLL$'|_{\rm NLO}$ cross sections with smaller R appears counterintuitive at first, given that the calculations entering the NLL$'|_{\rm NLO}$ expressions are performed in the narrow jet approximation, and correspondingly the agreement should improve at lower R. The increasing dependence on R at small R in the NLL$'|_{\rm NLO}$ expression is driven by the single logarithmic terms in R (or δ). Such terms can be resummed [44] which would reduce the δ-dependence of the predictions. Another improvement can be achieved by correcting in the hard function for effects of narrow jet approximation which at higher values of R might result in a percent-level correction, see e.g. [45].

Next, we discuss the resummed NLL$'$ results matched to the NLO predictions. From now, all matched NLO+NLL$'$ results discussed here, i.e. those shown in Figs. 5, 6 and 7, will contain information from the full set of partonic channels present at NLO. Fig. 4 presents differential distributions in Q. We find that the corrections beyond NLO taken into account in the resummed formula amount to up to 1%, depending on the value of Q. Inspecting the ratios of the NLO+NLL$'$ to NLO distributions, we also observe that the resummed corrections increase with growing Q. This behaviour is expected, as soft gluon corrections should be more pronounced closer to the threshold, approached with higher Q.

The upper panels of the two plots in Fig. 4 also show the scale variation uncertainty of the invariant mass distribution. The scale errors in the left plot are obtained by varying the factorization and renormalization scales simultaneously, $\mu = \mu_F = \mu_R$, between $Q/2$ and $2Q$. However, while simultaneous scale variation can provide a useful first indication on the size of the scale error, a more reliable estimate is usually obtained using the so-called 7-point method, where one considers $\left(\mu_R/\mu_{R,0}, \mu_F/\mu_{F,0}\right) \in \{(0.5, 0.5), (0.5, 1), (1, 0.5), (1, 1), (1, 2), (2, 1), (2, 2)\}$. In the right plot in Fig. 4 we show the scale error calculated with the 7-point method for $\mu_{R,0} = \mu_{F,0} = Q$. We see that while the NLO+NLL$'$ calculations lead to a visible reduction in the scale error at smaller values of Q in the left plot, the effect is smaller or even absent for the small-Q bins shown in the right plot, i.e. when the 7-point method is used to estimate the scale uncertainty.

Figure 5 shows the NLO+NLL$'$ and NLO total cross sections as functions of the scale ratio μ/μ_0 for $\mu_0 = Q$. We see that resummation provides a reduction of the scale dependence. The higher-order NLL$'$ corrections modify the absolute value of the total cross section at $\mu = \mu_0 = Q$ only minimally. Additionally, as demonstrated in Fig. 6, if the scale variation of results obtained

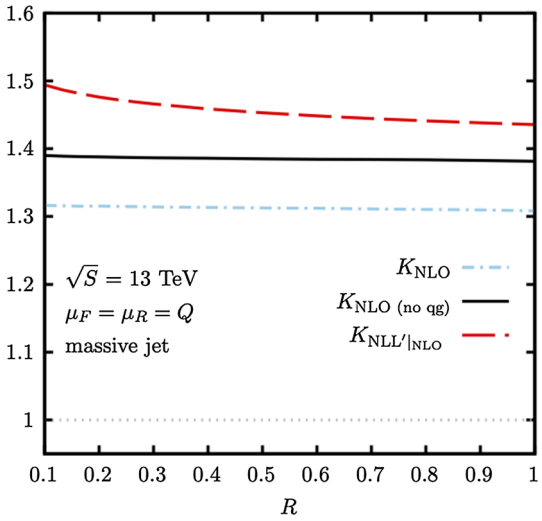

Fig. 3 Total K-factors as a function of R at $\mu = \mu_0 = Q$: ratios of the total cross sections calculated at the NLO, NLO (no qg) and NLL$'|_{\rm NLO}$ accuracy

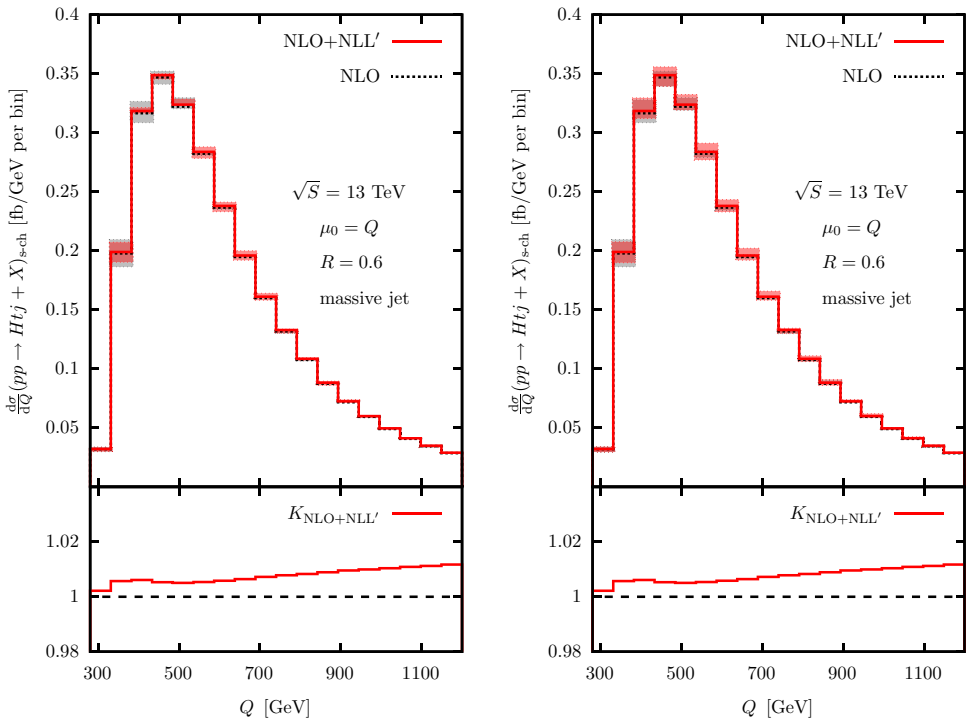

Fig. 4 Differential distributions in Q for massive jets for $R = 0.6$: (top) absolute values of the NLO, NLO+NLL$'$ distributions and (bottom) ratio of the NLO+NLL$'$ result to the NLO prediction. While the central values are the same in the left and right plots, the scale error shown in the left plot is obtained varying $\mu_F = \mu_R$ simultaneously, whereas the scale error in the right plot is obtained using a 7-point method

with various central scale choices is considered, the NLO+NLL$'$ results show much smaller spread in absolute values than the NLO results. This demonstrates the potential of resummation methods to increase the stability of the theoretical predictions and motivates further study of the subject.

For completeness, in Table 1 we provide, for various central scale choices, the central values of the cross sections at NLO and NLO+NLL' and the scale variation error obtained while varying $\mu_F = \mu_R$ between $Q/2$ and $2Q$. The information contained in Table 1 corresponds to (some of) the content of Figs. 5 and 6.

However, the dependence on the scale shown in Figs. 5 and 6, and the scale errors quoted in Table 1 have been obtained while varying μ_F and μ_R simultaneously. As already mentioned above, employing the 7-point method to estimate the scale error is expected to deliver a more reliable estimate of the error. Correspondingly, in Table 2 we present the central values of the total cross sections at NLO and NLO+NLL$'$ for various central scale choices, and the corresponding scale variation errors obtained using the 7-point method.[3] A graphical representation of the information in Table 2 is given in Fig. 7. In accordance with the result for the invariant mass distribution, we see that the 7-point method returns larger scale variation uncertainty than simultaneous variation of

[3] While the central values are exactly the same as those in Table 2, the values of the NLO errors are not the same but up to the accuracy shown in the tables, coincidentally return the same results.

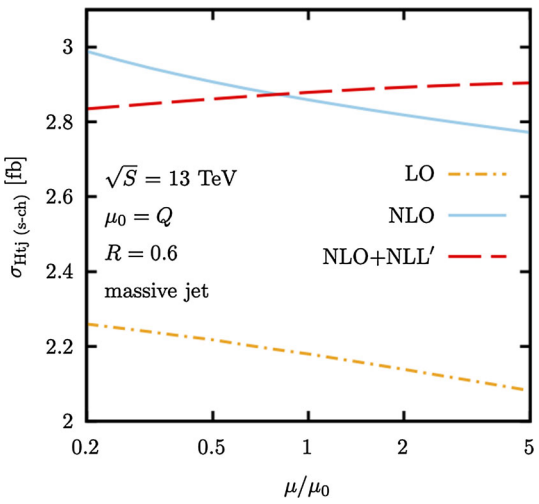

Fig. 5 Total cross section as a function of μ/μ_0 for $R = 0.6$ at the LO, NLO and the NLO+NLL′ accuracy

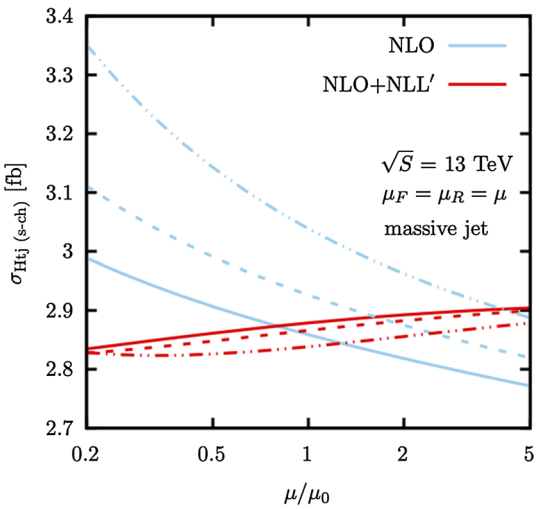

Fig. 6 Total cross section as a function of μ/μ_0 for $R = 0.6$ at the NLO and NLO+NLL′ accuracy. Results are shown for three central scale choices $\mu_0 = Q$ (solid lines), $\mu_0 = H_T/2$ (dashed lines), and $\mu_0 = H_T/6$ (dashed-dotted lines)

Table 1 Total cross sections at NLO and NLO+NLL′ accuracy for $R = 0.6$ with the scale error calculated varying μ_F and μ_R simultaneously.

μ_0	NLO [fb]	NLO+NLL′ [fb]
Q	$2.86^{+1.7\%}_{-1.4\%}$	$2.88^{+0.5\%}_{-0.6\%}$
$H_T/2$	$2.93^{+2.2\%}_{-1.8\%}$	$2.87^{+0.6\%}_{-0.4\%}$
$H_T/6$	$3.04^{+3.4\%}_{-2.5\%}$	$2.84^{+0.6\%}_{-0.6\%}$

μ_F and μ_R. The information in the figure and the table underlines the conclusion drawn on basis of the simultaneous scale variation results: while the impact of resummation on the central value of the total cross section, as well as the size of the scale error differs for various scale choices, resummation brings the central values closer together, significantly reducing a combined overall theoretical uncertainty.

Finally, we note that our expressions do not account for the contributions from non-global logarithms [46]. Such contributions are expected to appear when an observable is sensitive to radiation in only a limited sector of the phase space, which is the case for a jet defined using a certain jet radius parameter. In particular, they are known to arise in the massive jet case and their size has been studied in the context of dijet production in [47] or the boson-jet production in [48]. In fixed-order calculations they first appear in $\mathcal{O}(\alpha_s^2)$ corrections, while in regard to logarithmic orders they can contribute already at NLL. In this sense, they formally spoil the NLL accuracy claimed here. However, the studies performed so far in the literature indicate that their contribution is typically relatively small [47–49] making their resummation, e.g. along the lines of [50–52] beyond the scope of an exploratory study like this one.

Table 2 Total cross sections at NLO and NLO+NLL′ accuracy for $R = 0.6$ with the scale error calculated using the 7-point method

μ_0	NLO [fb]	NLO+NLL′ [fb]
Q	$2.86^{+1.7\%}_{-1.4\%}$	$2.88^{+2.2\%}_{-1.3\%}$
$H_T/2$	$2.93^{+2.2\%}_{-1.8\%}$	$2.87^{+2.0\%}_{-1.4\%}$
$H_T/6$	$3.04^{+3.4\%}_{-2.5\%}$	$2.84^{+1.6\%}_{-0.8\%}$

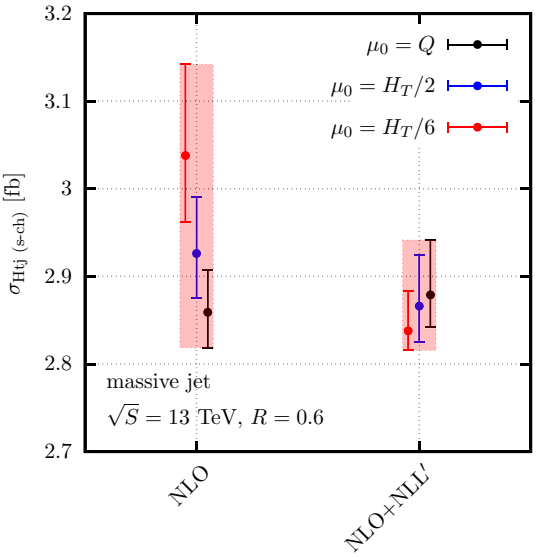

Fig. 7 Total cross sections at the NLO and NLO+NLL′ accuracy for $R = 0.6$ and three central scale choices $\mu_0 = Q$, $\mu_0 = H_T/2$, $\mu_0 = H_T/6$.

4 Summary

The NLO corrections to the *s*-channel *tHj* production are significant, at the level of 30%. The main contribution to them comes from the quark-initiated production channel, which indicates the importance of higher-order corrections in this channel. The work presented here focuses on exploring ways in which resummation methods in direct QCD resummation can be used to provide an estimate of the higher-order corrections. Of course, as the *tHj* production takes place only in the quark-antiquark channel at LO, the resummation corrections cannot be expected to be as important as for the process with gluons in the initial state. However, it is a formally well-defined set of higher-order corrections that can be systematically taken into account to all orders and studied numerically. The relevance of the measurement of the *tHj* process for gaining information on the top Yukawa coupling, as well as the increasing experimental precision make such studies more and more important with time.

In this exploratory work, we investigated a method of threshold resummation in direct QCD, set in the invariant mass kinematics and assuming nonzero jet mass. While we have shown that it is possible to obtain resummed predictions in this case by using Mellin space techniques, the definition of the threshold variable through the invariant mass of the final state system inevitably involves jet's momentum, leading to a residual dependence on a jet-size parameter R. Somewhat disappointingly, it also turns out that the pure soft gluon corrections at the invariant mass threshold, i.e. terms logarithmic in N, play a relatively small role for the process at hand. However, the scale dependence of our resummed predictions is visibly reduced in comparison with the NLO results. The improvement is particularly noticeable when different choices of the central scale value are additionally considered. This illustrates the potential of resummation methods to improve theoretical predictions for the *tHj* production. Our results also indicate that the calculations of the full higher-order corrections are very much needed in order to improve the description of the *tHj* production process.

Acknowledgements This work has been supported in part by the Deutsche Forschungsgemeinschaft (DFG) grant KU3103/2. V.T. acknowledges funding from the European Union's Horizon 2020 research and innovation programme as part of the Marie Skłodowska-Curie Innovative Training Network MCnetITN3 (grant agreement no. 722104), while L.M.V. acknowledges support from the DFG Research Training Group "GRK 2149: Strong and Weak Interactions - from Hadrons to Dark Matter".

Funding Open Access funding enabled and organized by Projekt DEAL.

Data Availability Statement The datasets generated during and/or analysed during the current study are available from the corresponding author on reasonable request.

References

1. F. Maltoni, K. Paul, T. Stelzer, S. Willenbrock, Phys. Rev. D **64**, 094023 (2001). [http://arxiv.org/abs/hep-ph/0106293 [hep-ph]]
2. T.M.P. Tait, C.P. Yuan, Phys. Rev. D **63**, 014018 (2000). [http://arxiv.org/abs/hep-ph/0007298 [hep-ph]]
3. G. Bordes, B. van Eijk, Phys. Lett. B **299**, 315–320 (1993)
4. V. Khachatryan et al., CMS. JHEP **06**, 177 (2016). [http://arxiv.org/abs/1509.08159 [hep-ex]]
5. A.M. Sirunyan *et al.* [CMS], Phys. Rev. D **99** (2019) no.9, 092005 [http://arxiv.org/abs/1811.09696 [hep-ex]]
6. G. Aad *et al.* [ATLAS], Eur. Phys. J. C **80** (2020) no.10, 957 [http://arxiv.org/abs/2004.03447 [hep-ex]]
7. G. Aad *et al.* [ATLAS], Phys. Rev. Lett. **125** (2020) no.6, 061802 [http://arxiv.org/abs/2004.04545 [hep-ex]]
8. A.M. Sirunyan *et al.* [CMS], [http://arxiv.org/abs/2011.03652 [hep-ex]]
9. F. Demartin, F. Maltoni, K. Mawatari, M. Zaro, Eur. Phys. J. C **75**, 6–267 (2015). [http://arxiv.org/abs/1504.00611 [hep-ph]]
10. C. Degrande, F. Maltoni, K. Mimasu, E. Vryonidou, C. Zhang, JHEP **10**, 005 (2018). [http://arxiv.org/abs/1804.07773 [hep-ph]]
11. D. Pagani, I. Tsinikos, E. Vryonidou, JHEP **08**, 082 (2020). [http://arxiv.org/abs/2006.10086 [hep-ph]]
12. A. Kulesza, L. Motyka, T. Stebel, V. Theeuwes, JHEP **1603**, 065 (2016). [http://arxiv.org/abs/1509.02780 [hep-ph]]
13. A. Kulesza, L. Motyka, T. Stebel, V. Theeuwes, PoS **LHCP2016** (2016), 084 [http://arxiv.org/abs/1609.01619 [hep-ph]]
14. A. Kulesza, L. Motyka, T. Stebel, V. Theeuwes, Phys. Rev. D **97** (2018) no.11, 114007 [http://arxiv.org/abs/1704.03363 [hep-ph]]
15. A. Kulesza, L. Motyka, D.Schwartländer, T. Stebel, V. Theeuwes, Eur. Phys. J. C **79** (2019) no.3, 249 [http://arxiv.org/abs/1812.08622 [hep-ph]]
16. A. Kulesza, L. Motyka, D. Schwartländer, T. Stebel, V. Theeuwes, Eur. Phys. J. C **80** (2020) no.5, 428 [http://arxiv.org/abs/2001.03031 [hep-ph]]
17. H.T. Li, C.S. Li, S.A. Li, Phys. Rev. D **90** (2014) 9, 094009 [http://arxiv.org/abs/1409.1460 [hep-ph]]
18. A. Broggio, A. Ferroglia, B.D. Pecjak, A. Signer, L.L. Yang, JHEP **1603**, 124 (2016). [http://arxiv.org/abs/1510.01914 [hep-ph]]
19. A. Broggio, A. Ferroglia, G. Ossola, B.D. Pecjak, JHEP **1609**, 089 (2016). [http://arxiv.org/abs/1607.05303 [hep-ph]]
20. A. Broggio, A. Ferroglia, B.D. Pecjak, L.L. Yang, JHEP **1702**, 126 (2017). [http://arxiv.org/abs/1611.00049 [hep-ph]]
21. A. Broggio, A. Ferroglia, G. Ossola, B.D. Pecjak, R.D. Sameshima, JHEP **04**, 105 (2017). [http://arxiv.org/abs/1702.00800 [hep-ph]]
22. A. Broggio, A. Ferroglia, R. Frederix, D. Pagani, B.D. Pecjak, I. Tsinikos, JHEP **08**, 039 (2019). [http://arxiv.org/abs/1907.04343 [hep-ph]]
23. M. Forslund, N. Kidonakis, Phys. Rev. D **102** (2020) no.3, 034006 [http://arxiv.org/abs/2003.09021 [hep-ph]]
24. M. Forslund, N. Kidonakis, [http://arxiv.org/abs/2103.01228 [hep-ph]]
25. D. de Florian, W. Vogelsang, Phys. Rev. D **76**, 074031 (2007). [http://arxiv.org/abs/0704.1677 [hep-ph]]
26. P. Hinderer, F. Ringer, G. Sterman, W. Vogelsang, Phys. Rev. D **99** (2019) no.5, 054019 [http://arxiv.org/abs/1812.00915 [hep-ph]]
27. X. Liu, S.O. Moch, F. Ringer, Phys. Rev. Lett. **119** (2017) no.21, 212001 [http://arxiv.org/abs/1708.04641 [hep-ph]]
28. N. Kidonakis, G. Oderda, G. Sterman, Nucl. Phys. B **525**, 299 (1998). [http://arxiv.org/abs/hep-ph/9801268]
29. H. Contopanagos, E. Laenen, G.F. Sterman, Nucl. Phys. B **484**, 303 (1997). (**[hep-ph/9604313]**)
30. N. Kidonakis, G. Oderda, G. Sterman, Nucl. Phys. B **531**, 365 (1998). [http://arxiv.org/abs/hep-ph/9803241]
31. R. Bonciani, S. Catani, M.L. Mangano, P. Nason, Phys. Lett. B **575**, 268 (2003). (**[hep-ph/0307035]**)
32. M. Furman, Nucl. Phys. B **197**, 413–445 (1982)
33. F. Aversa, M. Greco, P. Chiappetta, J.P. Guillet, Z. Phys. C **46**, 253 (1990)
34. B. Jager, M. Stratmann, W. Vogelsang, Phys. Rev. D **70**, 034010 (2004). [http://arxiv.org/abs/hep-ph/0404057 [hep-ph]
35. A. Mukherjee, W. Vogelsang, Phys. Rev. D **86**, 094009 (2012). [http://arxiv.org/abs/1209.1785 [hep-ph]]
36. J. Kodaira, L. Trentadue, Phys. Lett. B 112, 66, Phys. Lett. B **123**(1983), 335 (1982)
37. S. Catani, E. D'Emilio, L. Trentadue, Phys. Lett. B **211**, 335 (1988)
38. J. Alwall et al., JHEP **1407**, 079 (2014). [http://arxiv.org/abs/1405.0301[hep-ph]]
39. R.D. Ball, M. Bonvini, S. Forte, S. Marzani, G. Ridolfi, Nucl. Phys. B **874**, 746–772 (2013). [http://arxiv.org/abs/1303.3590 [hep-ph]]
40. M. van Beekveld, W. Beenakker, R. Basu, E. Laenen, A. Misra, P. Motylinski, Phys. Rev. D **100** (2019) no.5, 056009 [http://arxiv.org/abs/1905.11771 [hep-ph]]
41. S. Catani, M.L. Mangano, P. Nason, L. Trentadue, Nucl. Phys. B **478**, 273 (1996). [http://arxiv.org/abs/hep-ph/9604351]
42. M. Cacciari, G.P. Salam, G. Soyez, JHEP **04**, 063 (2008). [http://arxiv.org/abs/0802.1189 [hep-ph]]
43. S. Bailey, T. Cridge, L.A. Harland-Lang, A.D. Martin, R.S. Thorne, Eur. Phys. J. C **81** (2021) no.4, 341 [http://arxiv.org/abs/2012.04684 [hep-ph]]
44. M. Dasgupta, F.A. Dreyer, G.P. Salam, G. Soyez, JHEP **06**, 057 (2016). [http://arxiv.org/abs/1602.01110 [hep-ph]]
45. P. Sun, B. Yan, C.P. Yuan, F. Yuan, Phys. Rev. D **100** (2019) no.5, 054032 [http://arxiv.org/abs/1810.03804 [hep-ph]]
46. M. Dasgupta, G.P. Salam, Phys. Lett. B **512** (2001), 323-330 [http://arxiv.org/abs/hep-ph/0104277 [hep-ph]]
47. D. de Florian, P. Hinderer, A. Mukherjee, F. Ringer, W. Vogelsang, Phys. Rev. Lett. **112**, 082001 (2014). [http://arxiv.org/abs/1310.7192 [hep-ph]]
48. Y.T. Chien, D.Y. Shao, B. Wu, JHEP **11**, 025 (2019). [http://arxiv.org/abs/1905.01335 [hep-ph]]
49. T.T. Jouttenus, I.W. Stewart, F.J. Tackmann, W.J. Waalewijn, Phys. Rev. D **88** (2013) no.5, 054031 [http://arxiv.org/abs/1302.0846 [hep-ph]]
50. T. Becher, M. Neubert, L. Rothen, D.Y. Shao, JHEP **11** (2016), 019 [erratum: JHEP **05** (2017), 154] [http://arxiv.org/abs/1605.02737 [hep-ph]]
51. A.J. Larkoski, I. Moult, D. Neill, JHEP **09**, 143 (2015). [http://arxiv.org/abs/1501.04596 [hep-ph]]
52. A.J. Larkoski, I. Moult, D. Neill, JHEP **11**, 089 (2016). [http://arxiv.org/abs/1609.04011 [hep-ph]]
53. M.C. Kumar, S.O. Moch, Phys. Lett. B **730**, 122–129 (2014). [http://arxiv.org/abs/1309.5311 [hep-ph]]